



Signs of atmospheric inhomogeneities in cool stars from 1D-NLTE analysis of iron lines

L. Mashonkina¹, H.-G. Ludwig², A. Korn³, T. Sitnova¹, and E. Caffau²

¹ Institute of Astronomy, Russian Academy of Sciences, RU-119017 Moscow, Russia
e-mail: lima@inasan.ru

² Zentrum für Astronomie der Universität Heidelberg, Landessternwarte, Königstuhl 12,
D-69117 Heidelberg, Germany

³ Department of Physics and Astronomy, Division of Astronomy and Space Physics,
Uppsala University, Box 516, 75120 Uppsala, Sweden

Abstract. For the well studied halo star HD 122563 and the four stars in the globular cluster NGC 6397, we determine NLTE abundances of iron using classical plane-parallel model atmospheres. Each star reveals a discrepancy in abundances between the Fe I lines arising from the ground state and the other Fe I lines, in qualitative agreement with the 3D-LTE line formation predictions, however, the magnitude of the observed effect is a factor of 2 smaller compared with the predicted one. When ignoring the Fe I low-excitation lines, the NLTE abundances from the two ionization stages, Fe I and Fe II, are consistent in each investigated star. For the subgiants in NGC 6397, this is only true when using the cooler effective temperature scale of Alonso et al. (1999). We also present full 3D-LTE line formation calculations for some selected iron lines in the solar and metal-poor 4480/2/-3 models and NLTE calculations with the corresponding spatial and temporal average ⟨3D⟩ models. The use of the ⟨3D⟩ models is justified only for particular Fe I lines in particular physical conditions. Our NLTE calculations reproduce well the centre-to-limb variation of the solar Fe I 7780 Å line, but they are unsuccessful for Fe I 6151 Å. The metal-poor ⟨3D⟩ model was found to be adequate for the strong Fe I 5166 Å ($E_{\text{exc}} = 0$) line, but inadequate in all other investigated cases.

Key words. Line: formation – Stars: abundances – Stars: atmospheres

1. Introduction

Most stellar-parameters and chemical-abundance studies of cool stars still employ classical plane-parallel (1D) model atmospheres. How large are the abundance errors caused by ignoring hydrodynamical phenom-

ena (3D effects) in the atmosphere of such stars? Collet et al. (2007) published (3D-1D) abundance corrections for some fictitious Fe I and Fe II lines in a small grid of model atmospheres representing the atmosphere of cool giants of various metallicities. These data were updated by Hayek et al. (2011) by including Rayleigh scattering in the line-

Send offprint requests to: L. Mashonkina

formation calculations. Significant changes were found only for the ultra-violet lines, with a wavelength of 3000 Å. Therefore, for the lines lying in the visual spectral range, we cite hereafter the more extensive calculation of Collet et al. (2007).

They showed that the 3D corrections are negative for the low-excitation ($E_{\text{exc}} \leq 2$ eV) lines of Fe I independent of their strength in the $[\text{Fe}/\text{H}] = -2$ and -3 models. The magnitude of the correction depends strongly on excitation energy of the lower level. For example, in the $T_{\text{eff}}/\log g/[\text{Fe}/\text{H}] = 5035/2.2/-2$ model, the (3D-1D) correction is slightly negative for the $E_{\text{exc}} = 4$ and 5 eV lines, but it goes down to -0.6 dex for the $E_{\text{exc}} = 0$ lines. The magnitude of correction increases towards lower metallicity. Classical abundance analysis of metal-poor (MP) stars should reveal an abundance difference of 0.5 dex between different excitation Fe I lines if the theoretical predictions of Collet et al. (2007) are correct.

The theory predicts positive corrections for the Fe II lines. For example, (3D-1D) = $+0.2$ dex for the $E_{\text{exc}} = 3$ eV lines in the 5035/2.2/-2 model. With 3D effects having opposite sign for Fe I and Fe II lines, rather large shifts to stellar surface gravities should result from spectroscopic analyses. This is worrisome given the overall decent agreement between spectroscopic analyses and stellar parameters from stellar-structure models.

This study carefully checks the iron lines in the few MP stars with well determined stellar parameters using classical 1D model atmospheres and non-local thermodynamical equilibrium (NLTE) line formation. We are interested in uncovering any discrepancies between Fe I and Fe II and between Fe I lines of different excitation energy and to evaluate their magnitude if they exist. The obtained results are presented in Sect. 3.

At present, there are no tools to perform full 3D-NLTE line formation calculations for atoms with a complicated term structure like those of Fe I and Fe II. The full 3D line-formation calculations differ from their 1D counterparts due to different mean atmospheric structures and the existence of atmospheric inhomogeneities. The effect of different mean at-

mospheric structures on emergent fluxes and derived chemical abundances can be evaluated using the spatially and temporally averaged atmospheric stratification denoted ⟨3D⟩. We investigate here how closely the ⟨3D⟩ line formation for iron resembles that of the corresponding full 3D model. Section 4 compares the observed solar centre-to-limb variation of some Fe I lines with the predictions from the ⟨3D⟩ NLTE line-formation modelling. The LTE and NLTE calculations were also performed with the average 3D models representing the atmospheres of very metal-poor (VMP) cool giants (see Sect. 5). Our conclusions are given in Sect. 6.

2. Method of calculations

The statistical equilibrium of Fe I-Fe II was calculated with a comprehensive model atom using the method of Mashonkina et al. (2011) and the code DETAIL (Butler & Giddings 1985), where the opacity package was updated. Inelastic collisions with H I atoms were taken into account employing the classical Drawinian rates scaled by a factor $S_{\text{H}} = 0.1$. The line profile calculations were performed with the code SIU (Reetz 1991).

For classical 1D model atmospheres, we used the MARCS grid (Gustafsson et al. 2008) and the model 4600/1.6/-2.5 computed with the code MAFAGS-OS (Grupp et al. 2009). The 3D model atmospheres were computed with the code CO⁵BOLD (Freytag et al. 2012). The average ⟨3D⟩ models were obtained by horizontally averaging each 3D snapshot over surfaces of equal (Rosseland) optical depth. For comparison, we also considered the 1D hydrostatic mixing-length model atmospheres which employ the same micro-physics and radiative transfer scheme as CO⁵BOLD. They are referred to as 1D_{LHD} models.

In this study, we determined absolute stellar iron abundances based on the linelist provided by Mashonkina et al. (2011). However, only the iron lines with accurate atomic data available were included in the analysis. For Fe I, we selected the lines with gf -values measured by either the Oxford or Hannover group. The two different sets of gf -values were ap-

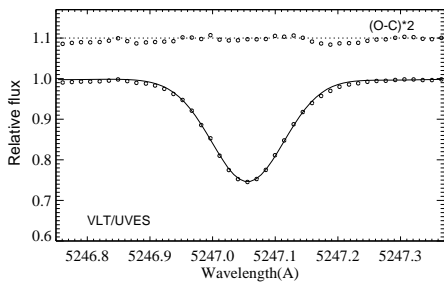


Fig. 1. The best fit (continuous curve) of the Fe I 5247 Å line in HD 122563 (open circles) obtained from the NLTE calculations with the MAFAGS-OS model 4600/1.60/−2.5. The theoretical profile was convolved with a profile that combines instrumental broadening with a Gaussian profile of 3 km^{−1} and broadening by macroturbulence with a radial-tangential profile of 4 km^{−1}. The differences between observed and calculated spectra (O - C) multiplied by a factor of 2 are presented in the upper part of figure (offset by +1.1).

plied for Fe II. One is of Meléndez & Barbuy (2009, hereafter, MB09), and another is of Raassen & Uylings (1998, hereafter, RUM). The RUM *gf*-values were corrected by a factor +0.11 dex following the recommendation of Grevesse & Sauval (1999).

3. 1D-NLTE analysis of iron lines in some selected metal-poor stars

3.1. VMP cool giant HD 122563

HD 122563 was selected as one of the best observed halo stars, with well determined stellar parameters. Recent measurements of its angular diameter (Creevey et al. 2012) give $T_{\text{eff}} = 4600 \pm 41$ K. In our earlier paper (Mashonkina et al. 2011), we employed the same value, which was based on empirical colour calibrations, to calculate the gravity $\log g = 1.60 \pm 0.07$ from the HIPPARCOS parallax.

A high-quality spectrum of HD 122563 ($R \simeq 80\,000$ and $S/N > 200$) was taken from the ESO UVESPOP survey (Bagnulo et al. 2003). The quality of line profile fits is illustrated in Fig. 1 for Fe I 5247 Å.

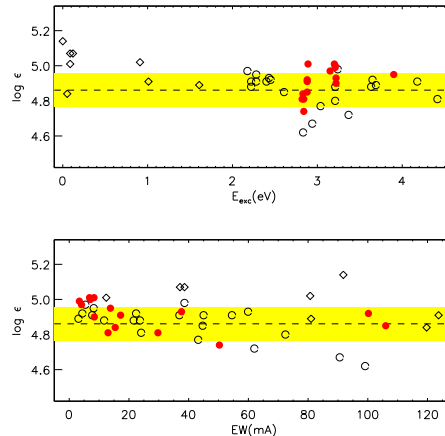


Fig. 2. NLTE ($S_{\text{H}} = 0.1$) abundances derived from the Fe I (open circles for $E_{\text{exc}} \geq 2$ eV and rombs for $E_{\text{exc}} < 2$ eV) and Fe II (filled circles) lines in HD 122563 as a function of excitation energy of the lower level (top panel) and observed equivalent width (bottom panel). In each panel, the dashed line shows the mean iron abundance determined from the Fe I $E_{\text{exc}} \geq 2$ eV lines.

The NLTE abundances derived from individual lines in HD 122563, in total, from 29 lines of Fe I and 15 lines of Fe II, are presented in Fig. 2. We adopted the microturbulence velocity $\xi_t = 1.95$ km^{−1} as determined by Mashonkina et al. (2011) from Fe I and Fe II lines. Interestingly, the use of different sets of *gf*-values leads to very similar mean abundances from the Fe II lines, i.e., $\log \varepsilon_{\text{FeII}}(\text{MB09}) = 4.92 \pm 0.08$ and $\log \varepsilon_{\text{FeII}}(\text{RUM}) = 4.91 \pm 0.09$. When calculating the mean abundance from the Fe I lines, we included only those with $E_{\text{exc}} \geq 2$ eV, which are predicted to be less affected by 3D effects. In NLTE ($S_{\text{H}} = 0.1$), we find consistent abundances between Fe I and Fe II, with the difference $(\text{Fe I}(\geq 2 \text{ eV}) - \text{Fe II})_{\text{NLTE}} = -0.06$ dex, when using the MB09 *gf*-values. In contrast, the difference between the corresponding LTE abundances amounts to −0.26 dex. We note that the Fe I lines arising from the ground term ($E_{\text{exc}} < 0.2$ eV) reveal, on average, a 0.2 dex higher abundance compared to that of the remaining Fe I lines.

Collet et al. (2009) determined the LTE abundances from individual Fe I and Fe II lines in HD 122563 based on full 3D line-formation calculations. The stellar parameters employed were the same as in our study. For the Fe I lines, Collet et al. (2009) found negative 3D abundance corrections, which depend strongly on the lower-level excitation potential. For example, $(3D - 1D) \simeq -0.3$ for $E_{\text{exc}} = 3$ eV. In contrast, they obtained approximately 0.4 dex higher 3D than 1D abundances from the Fe II lines. Collet et al. (2009) argued that “such trends may be attributed to the neglected departures from LTE in the spectral line-formation calculations”.

When applying the 3D corrections of Collet et al. (2009) to our NLTE abundances, we obtain a dramatic discrepancy between Fe I and Fe II, with $(\text{Fe I}(\geq 2 \text{ eV}) - \text{Fe II})_{\text{NLTE}+3\text{D}} = -0.75$ dex.

As for the Fe I lines arising from the ground state, 3D acts in right direction, but the predicted magnitude -0.8 dex of the 3D correction is markedly too large.

3.2. Subgiants and red giants of NGC 6397

Our analysis was extended to higher temperatures and higher gravities by inspecting the iron abundances of stars in the globular cluster (GC) NGC 6397 on high-quality ($R \simeq 47000$, $S/N \simeq 100$) spectra taken with the FLAMES-UVES spectrograph at the Very Large Telescope (see Korn et al. 2007, for a detailed description of the observations). We selected the two stars N5281 and N8298 on the subgiant branch (SGB) and the two stars N11093 and N14592 on the red giant branch (RGB). Stellar parameters of these stars were discussed in detail by Nordlander et al. (2012). Here, we employ the photometric effective temperatures deduced from two different empirical colour calibrations of Casagrande et al. (2010) and Alonso et al. (1999) for dwarfs and those from calibrations of Alonso et al. (1996) for giants. Following Nordlander et al. (2012), we consider the SGB stars to belong to the dwarf calibration. It is worth noting that the calibrations of Casagrande et al.

(2010) are also valid for subgiants. The accurate determination of surface gravity of the GC stars takes advantage of their common distance that can be evaluated from the comparison of the observed and theoretical colour-magnitude diagrams. The gravity was computed from the usual relation between $\log g$ and L , T_{eff} , and mass of the observed stars. The used stellar parameters are indicated in Table 1. Microturbulence velocities were derived from Fe II lines by Korn et al. (2007).

The element abundances determined from individual iron lines turn out very similar for each pair of the SGB and RGB stars. As in HD 122563, the Fe I lines arising from the ground term give higher abundances compared to those from the other Fe I lines, by 0.18 dex and 0.20 dex, on average, for the SGB and RGB stars, respectively. Therefore, mean Fe I based abundances were computed ignoring the low-excitation ($E_{\text{exc}} < 2$ eV) lines of Fe I. In contrast to HD 122563, we find differences of 0.06 dex and 0.04 dex for the SGB and RGB stars, respectively, in mean abundance derived from the Fe II lines between applying gf -values from RUm and MB09. This is due to the smaller number of lines measured in the GC stars. Table 1 presents the obtained results.

We find that the NLTE ($S_{\text{H}} = 0.1$) abundances determined from two ionization stages are consistent within the error bars in the RGB stars, when using the RUm gf -values, with $(\text{Fe I} - \text{Fe II})_{\text{NLTE}} = 0.07$ dex and 0.02 dex for N11093 and N14592, respectively. In LTE, the corresponding differences amount to -0.11 dex and -0.16 dex. For the SGB stars, a discrepancy in NLTE abundances between Fe I and Fe II does not exceed 1σ when employing the T_{eff} scale of Alonso et al. (1999) and the RUm gf -values, but increases significantly for the hotter temperature $T_{\text{eff}} = 5978$ K based on the Casagrande et al. (2010) calibrations.

When applying the 3D corrections presented by Korn et al. (2007), we come to large discrepancy between Fe I and Fe II not only in LTE, but also in NLTE, namely, $(\text{Fe I} - \text{Fe II})_{\text{NLTE}+3\text{D}}$ is equal -0.2 dex, on average, for the two RGB stars, -0.2 dex and -0.1 dex for the SGB stars on the T_{eff} scale of Alonso

Table 1. Iron abundances $\log \varepsilon$ and abundance differences $\Delta = \text{Fe I} - \text{Fe II}$ for the stars in NGC 6397

Star	T_{eff} K	$\log g$	ξ_t kms ⁻¹	LTE		NLTE		
				Fe I	Fe II	Fe I	Fe II	Δ
	IRFM 2010 ¹							
N5281	5978	3.73	1.75	5.31 \pm 0.07 (15)	5.34 ⁵ \pm 0.07 (6)	5.52 \pm 0.07	5.34 ⁵ \pm 0.07	0.18
N8298	5978	3.73	1.75	5.31 \pm 0.06 (15)	5.36 ⁵ \pm 0.03 (6)	5.52 \pm 0.06	5.36 ⁵ \pm 0.03	0.16
	IRFM 1999 ²							
N5281	5816	3.69	1.75	5.19 \pm 0.08	5.25 ⁴ \pm 0.09	5.38 \pm 0.08	5.25 ⁴ \pm 0.09	0.13
N5281	5816	3.69	1.75		5.31 ⁵ \pm 0.07		5.31 ⁵ \pm 0.07	0.07
N8298	5816	3.69	1.75	5.19 \pm 0.06	5.27 ⁴ \pm 0.09	5.39 \pm 0.06	5.27 ⁴ \pm 0.09	0.12
N8298	5816	3.69	1.75		5.33 ⁵ \pm 0.03		5.33 ⁵ \pm 0.03	0.06
	IRFM 1996 ³							
N11093	5100	2.51	1.7	5.09 \pm 0.10 (15)	5.16 ⁴ \pm 0.10 (9)	5.27 \pm 0.10	5.16 ⁴ \pm 0.10	0.11
N11093	5100	2.51	1.7		5.20 ⁵ \pm 0.06		5.20 ⁵ \pm 0.06	0.07
N14592	5120	2.58	1.6	5.09 \pm 0.08 (15)	5.21 ⁴ \pm 0.09 (9)	5.27 \pm 0.09	5.21 ⁴ \pm 0.09	0.06
N14592	5120	2.58	1.6		5.25 ⁵ \pm 0.05		5.25 ⁵ \pm 0.05	0.02

Notes. Numbers in brackets indicate the total number of lines used in calculating the mean.

¹ T_{eff} is based on calibrations of Casagrande et al. (2010) for dwarfs and subgiants,

² T_{eff} is based on calibrations of Alonso et al. (1999) for dwarfs,

³ T_{eff} is based on calibrations of Alonso et al. (1996) for giants,

⁴ based on gf -values of MB09; ⁵ based on gf -values of RUM.

et al. (1999) and Casagrande et al. (2010), respectively.

The above results may cast a shadow of doubt on 3D calculations. However, our interpretation is that one cannot simply add 1D-NLTE and 3D-LTE results when both NLTE and 3D effects are significant. Exactly this is the case in metal-poor stars.

4. Centre-to-limb variation of solar Fe I lines

At present, one cannot perform full 3D and NLTE line-formation calculations for iron due to its complex atomic structure. In this section, we investigate whether NLTE calculations coupled to average $\langle 3D \rangle$ models can reproduce observations of the centre-to-limb variation of the solar Fe I 7780 Å and 6151 Å lines. The measured equivalent widths (EW) were taken from Pereira et al. (2009). We apply the CO⁵BOLD solar 3D and average $\langle 3D \rangle$ models and also

the MAFAGS-OS solar 1D model. When computing the theoretical EW , the iron abundance has been adjusted so that the models fit the observations at disk-centre. For the $\langle 3D \rangle$ and 1D model atmospheres, all the line profiles were computed with a microturbulence of $\xi_t = 0.9 \text{ kms}^{-1}$.

The obtained results are presented in Fig. 3. It is evident that the classical model atmosphere fails to reproduce the observations. We do not show the NLTE results for the 1D model because NLTE leads to weakened Fe I lines and larger discrepancy between the theory and observations. The NLTE calculations with the $\langle 3D \rangle$ model reproduce nearly perfectly the behavior of Fe I 7780 Å, but the $\langle 3D \rangle$ model is unsuccessful in the case of Fe I 6151 Å, both in LTE and NLTE. Full 3D-LTE line-formation calculations correctly predict the growth of $EW(\text{Fe I } 6151 \text{ Å})$ toward the limb, albeit with overestimated theoretical EW s. The latter can

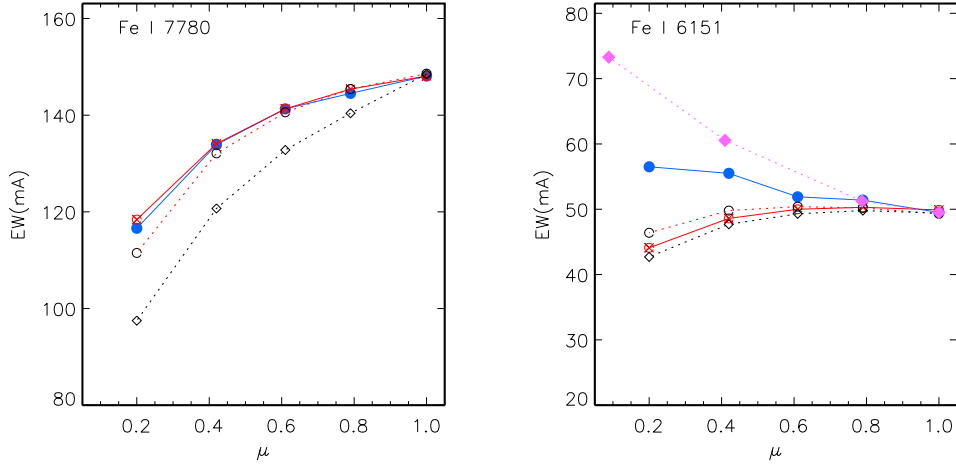


Fig. 3. Solar observed (filled circles) and predicted centre-to-limb variations of line equivalent widths for Fe I 7780 Å (left panel) and Fe I 6151 Å (right panel). Filled rombs (only for Fe I 6151 Å) correspond to full 3D-LTE line formation, crossed open circles to the NLTE calculations with the $\langle 3D \rangle$ model, open circles to LTE with $\langle 3D \rangle$, and open rombs to LTE with the MAFAGS-OS model.

be due to neglecting the departures from LTE for Fe I.

These results illustrate the varying sensitivity of different Fe I lines to 3D effects. The Fe I 7780 Å line seems to be mostly affected by the change in mean atmospheric structure of 3D compared with 1D model, while Fe I 6151 Å is more sensitive to atmospheric inhomogeneity.

5. Test calculations with metal-poor average $\langle 3D \rangle$ models

It would be useful to produce a list of lines that are more sensitive to the change in mean atmospheric structure than to atmospheric inhomogeneity. Such lines could be reliably employed in stellar abundance analyses with $\langle 3D \rangle$ models. In this section, we check three lines of Fe I and Fe II 5018 Å line in the full 3D, average $\langle 3D \rangle$, and reference 1D models of VMP cool giant with $T_{\text{eff}} = 4480$ K, $\log g = 2$, and $[M/H] = -3$. The results are presented in Table 2 as the differences in abundance derived for a given line equivalent width between different models.

Despite the low iron abundance, all the selected lines are rather strong, with EW from

70 mÅ to 95 mÅ. The full 3D-LTE line-formation calculations show that the effect of atmospheric inhomogeneity is weak only for Fe I 5166 Å (the row 3D - $\langle 3D \rangle$ in Table 2, part I). In contrast, Fe I 5232 Å and Fe II 5018 Å are mostly affected by horizontal temperature/pressure fluctuations. To examine a dependence of the 3D effects on the line strength, the calculations were also performed with gf -values reduced by one order of magnitude (Table 2, part II). The results differ dramatically: 3D effects are significantly reduced for Fe I 5232 Å and Fe II 5018 Å and, in contrast, are enhanced for the low-excitation lines, Fe I 5166 Å and Fe I 4994 Å. In the case labelled "weak lines", all lines are predominantly affected by atmospheric inhomogeneities (the row 3D - $\langle 3D \rangle$ in Table 2, part II). An exception is Fe I 5232 Å, with its minor (3D - $\langle 3D \rangle$) correction.

We also performed LTE and NLTE calculations with various kinds of averaged 3D models. The full 3D model was decomposed into 12 groups depending on the emergent intensity. The fraction of surface area with given intensity defines the weight of the corresponding group. By spatially and temporally averaging

Table 2. Abundance differences (dex) between different 4480/2/−3 models

Line:	Fe I 5166	Fe I 4994	Fe I 5232	Fe II 5018	
E_{exc} (eV):	0.0	0.9	2.9	2.9	
$\log gf$:	−4.20	−2.96	−0.06	−1.24	
<hr/>					
I. “strong lines”	$EW(\text{m}\text{\AA})$:	80	75	95	70
3D - 1D _{LHD}	LTE	−0.22	−0.04	+0.29	+0.50
3D - ⟨3D⟩		−0.02	+0.08	+0.35	+0.43
⟨3D⟩ ₁₂ - 1D _{LHD}	NLTE	0.00	+0.06	+0.15	+0.10
	LTE	−0.22	−0.14	−0.02	+0.10
⟨3D⟩ ₁₂ - ⟨3D⟩	NLTE	+0.03	+0.04	+0.05	+0.02
	LTE	−0.05	−0.04	−0.01	+0.02
⟨3D⟩ - 1D _{LHD}	NLTE	−0.07	−0.01	+0.10	+0.09
	LTE	−0.16	−0.09	−0.01	+0.08
<hr/>					
II. “weak lines”	$EW(\text{m}\text{\AA})$:	25	20	35	30
3D - 1D _{LHD}	LTE	−0.39	−0.23	+0.02	+0.20
3D - ⟨3D⟩		−0.30	−0.20	−0.02	+0.13
⟨3D⟩ ₁₂ - 1D _{LHD}	NLTE	+0.04	+0.08	+0.13	+0.10
	LTE	−0.15	−0.08	+0.04	+0.10
⟨3D⟩ ₁₂ - ⟨3D⟩	NLTE	+0.03	+0.04	+0.05	+0.02
	LTE	−0.09	−0.06	−0.02	+0.02
⟨3D⟩ - 1D _{LHD}	NLTE	+0.01	+0.04	+0.09	+0.08
	LTE	−0.06	−0.01	+0.06	+0.09

each group we obtained the 12 average group models. The theoretical emergent line fluxes from all the average group models were integrated using the group weights. The obtained results are hereafter referred to as $\langle 3D \rangle_{12}$.

In Fig. 4, we compare the Fe I 5166 Å line fluxes from different models in the “weak line” case. In LTE, the line is stronger in the $\langle 3D \rangle_{12}$ model than in the $\langle 3D \rangle$ and 1D ones. In NLTE, the 3D effects are weakened and the $\langle 3D \rangle$ model approaches the $\langle 3D \rangle_{12}$ one. In the “strong line” case, the difference ($\langle 3D \rangle_{12}$ - 1D_{LHD}) in LTE abundance is identical to (3D - 1D_{LHD}) for this line. The $\langle 3D \rangle_{12}$ model seems to simulate the 3D model better than the $\langle 3D \rangle$ model for the lines affected mostly by the change in mean atmospheric structure.

As for the remaining lines under the LTE assumption, both $\langle 3D \rangle_{12}$ and $\langle 3D \rangle$ models are inadequate for Fe II 5018 Å and for Fe I 5232 Å in the “strong lines” case. The 3D effects are, in part, reproduced by the $\langle 3D \rangle_{12}$ and $\langle 3D \rangle$ models for Fe I 4994 Å.

We find that the NLTE effects for each Fe I line are stronger in the $\langle 3D \rangle_{12}$ model than $\langle 3D \rangle$ and 1D ones. Only in the “strong line” case of Fe I 5166 Å, where the $\langle 3D \rangle_{12}$ model is working, the 3D effects are fully compensated by the NLTE effects, and no difference in NLTE abundances was obtained between $\langle 3D \rangle_{12}$ and 1D models.

We caution against simple adding the 1D-NLTE and 3D-LTE corrections to obtain the correction to the abundance derived from classical 1D-LTE analysis. For example, for the “strong” Fe I 5166 Å line in the 4480/2/−3 model, we calculated (3D - 1D) = −0.22 dex under the LTE assumption. The NLTE correction computed with the 1D model amounts to $\Delta_{\text{NLTE}} = \log \epsilon_{\text{NLTE}} - \log \epsilon_{\text{LTE}} = 0.16$ dex. Their adding results in a combined correction of −0.06 dex, while we see no difference in NLTE abundances between $\langle 3D \rangle_{12}$ and 1D models. When applying $\Delta_{\text{NLTE}} = 0.24$ dex as computed with the $\langle 3D \rangle$ model, the combined NLTE and 3D correction is +0.02 dex. Therefore, the use of the average 3D model can be helpful, how-

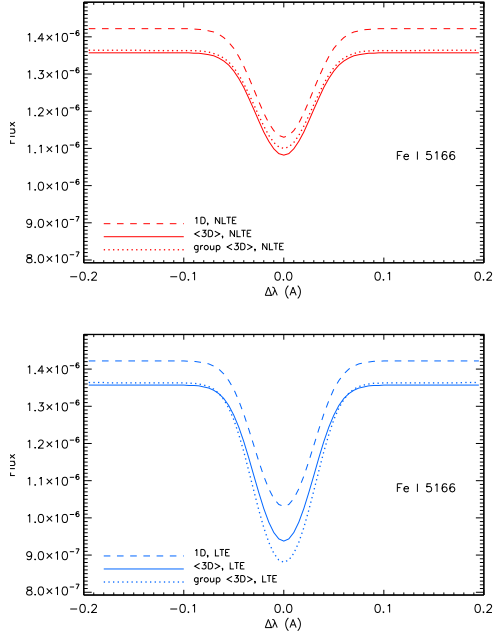


Fig. 4. Theoretical NLTE (top panel) and LTE (bottom panel) fluxes (in $\text{erg cm}^{-2} \text{s}^{-1} \text{Hz}^{-1}$) for Fe I 5166 Å from the $\langle 3D \rangle_{12}$ (dotted curve), $\langle 3D \rangle$ (continuous curve), and $1D_{\text{LHD}}$ (dashed curve) models 4480/2/-3. All the computations were performed with $\log g_f = -5.2$ and $\xi_t = 1.8 \text{ km s}^{-1}$.

ever, we stress, only when the 3D effects are mainly caused by the change in mean atmospheric structure.

6. Conclusions

We summarize our findings as follows.

1. To within the error bars, consistent NLTE abundances were obtained from the two ionization stages, Fe I and Fe II, for the stars with well determined stellar parameters HD 122563 and red giants in NGC 6397 using classical plane-parallel model atmospheres.
2. For HD 122563 and the stars in NGC 6397, the Fe I lines arising from the ground term reveal approximately 0.2 dex higher abundances compared to those from other Fe I lines. The obtained discrepancy between

lines of different excitation lines cannot be explained by using the 3D corrections of Collet et al. (2007) and Hayek et al. (2011). The 3D corrections predicted for the low-excitation Fe I lines are markedly too large.

3. The use of the average $\langle 3D \rangle$ models is justified for particular Fe I lines with the 3D effects mainly caused by the change in mean atmospheric structure of the 3D model compared to the 1D one. Our NLTE calculations reproduce well the centre-to-limb variation of the solar Fe I 7780 Å line, but they are unsuccessful for Fe I 6151 Å. The metal-poor $\langle 3D \rangle$ model was found to be adequate for the “strong” Fe I 5166 Å ($E_{\text{exc}} = 0$) line, but inadequate for the lines sensitive to atmospheric inhomogeneities, i.e., Fe I 5232 Å, Fe I 4994 Å and Fe II 5018 Å.
4. For Fe I, departures from LTE are expected to be stronger in 3D models than in 1D ones.
5. Simply adding 1D-NLTE and 3D-LTE corrections to the abundances determined from classical LTE analysis does not provide 3D-NLTE results.

Consistent 3D and NLTE line formation modelling is highly desirable for iron lines in metal-poor stars.

Acknowledgements. L. M. is supported by the DFG Sonderforschungsbereich (SFB) 881, “The Milky Way System” and the Presidium RAS Programme “Non-stationary phenomena in the Universe”. H.-G. L. is supported by the DFG SFB 881 (subproject A4). A. J. K. is supported by the Swedish National Space Board (SNSB) and the European Science Foundation (ESF). T. S. is supported by the Russian Federal Agency on Science and Innovation (grant 8394, 20.08.2012)

References

- Alonso, A., Arribas, S., & Martínez-Roger, C. 1996, *A&A*, 313, 873
 Alonso, A., Arribas, S., & Martínez-Roger, C. 1999, *A&AS*, 140, 261
 Bagnulo, S., Jehin, E., Ledoux, C., et al. 2003, *The Messenger*, 114, 10
 Butler, K. & Giddings, J. 1985, *Newsletter on the analysis of astronomical spectra*, No. 9, University of London

- Casagrande, L., Ramírez, I., Meléndez, J., Bessell, M., & Asplund, M. 2010, *A&A*, 512, A54
- Collet, R., Asplund, M., & Trampedach, R. 2007, *A&A*, 469, 687
- Collet, R., Nordlund, Å., Asplund, M., Hayek, W., & Trampedach, R. 2009, *Mem. Soc. Astron. Italiana*, 80, 719
- Creevey, O. L., Thévenin, F., Boyajian, T. S., et al. 2012, *A&A*, 545, A17
- Freytag, B., Steffen, M., Ludwig, H.-G., et al. 2012, *Journal of Computational Physics*, 231, 919
- Grevesse, N. & Sauval, A. J. 1999, *A&A*, 347, 348
- Grupp, F., Kurucz, R. L., & Tan, K. 2009, *A&A*, 503, 177
- Gustafsson, B., Edvardsson, B., Eriksson, K., et al. 2008, *A&A*, 486, 951
- Hayek, W., Asplund, M., Collet, R., & Nordlund, Å. 2011, *A&A*, 529, A158
- Korn, A. J., Grundahl, F., Richard, O., et al. 2007, *ApJ*, 671, 402
- Mashonkina, L., Gehren, T., Shi, J.-R., Korn, A. J., & Grupp, F. 2011, *A&A*, 528, A87
- Meléndez, J. & Barbuy, B. 2009, *A&A*, 497, 611
- Nordlander, T., Korn, A. J., Richard, O., & Lind, K. 2012, *ApJ*, 753, 48
- Pereira, T. M. D., Asplund, M., & Kiselman, D. 2009, *A&A*, 508, 1403
- Raassen, A. J. J. & Uylings, P. H. M. 1998, *A&A*, 340, 300
- Reetz, J. K. 1991, Diploma Thesis (Universität München)